Interdisciplinary Research in Medical Sciences Specialty
ISSN: 3062-4401
2025, Volume 5, Issue 1, Page No: 42-56

Available online at: www.galaxypub.co/page/journals

Galaxy Publication

Next-Generation Anti-Adhesive Medical Devices: Leveraging Plasma-Grown Nanostructured Silver for Biofilm Prevention

Henrique Silva[1], André Pinto[1], Vasco Neves[1]*

[1]Department of Health Technology, Faculty of Medicine, University of Aveiro, Aveiro, Portugal.

***E-mail** ✉ vasco.neves.ht@outlook.com

Received: 11 October 2024; **Revised:** 14 January 2025; **Accepted:** 16 January 2025

ABSTRACT

Biofilm accumulation on implantable silicone-based medical devices remains a critical challenge for healthcare systems. To address this, we introduce a novel, multi-modal strategy to preemptively inhibit bacterial colonization. This study investigates the efficacy of plasma-synthesized nanostructured metallic silver coatings—specifically three distinct geometries termed “Sharp blades,” “Thick blades,” and “Leaves”—immobilized onto stretchable substrates via a plasma-polymerized penta-fluorophenyl methacrylate thin film. Crucially, these coatings leverage a synergistic mechanism: the combination of inherent silver bacteriophobicity with the surface’s superhydrophobic topography creates a profound physical impediment to initial bacterial attachment. The bacteriophobic performance, which is tunable by controlling the plasma polymerization parameters of the underlying polymer, was rigorously characterized using FE-SEM, live/dead staining, and direct adhesion counts across various bacterial strains. The results demonstrate a remarkable reduction in bacterial adhesion by up to six orders of magnitude compared to bare surfaces, establishing this plasma-mediated nanostructuring as a highly effective, non-leaching methodology for engineering next-generation, biofilm-resistant medical materials.

Keywords: Nanostructure, Biofilm, Surface characterization, Bacteriophobic surfaces, Metallic silver

How to Cite This Article: Silva H, Pinto A, Neves V. Next-Generation Anti-Adhesive Medical Devices: Leveraging Plasma-Grown Nanostructured Silver for Biofilm Prevention. Interdiscip Res Med Sci Spec. 2025;5(1):53-56. https://doi.org/10.51847/vTocMgfDlu

Introduction

Health Care-Associated Infections (HCAIs), typically emerging after 48 hours of hospitalization, present a persistent and critical threat, with over 80% of cases linked to the implantation of medical devices. The root of this clinical challenge is biofilm formation—a process initiated by the adhesion of bacteria to the device surface, followed by the excretion of an extracellular matrix that establishes a consolidated, durable structure. These biofilms not only confer high levels of resistance against standard antibiotics and biocides but also force healthcare toward a challenging ‘post-antibiotic era.’

In response, therapeutic efforts have pivoted toward modifying the medical device surface to incorporate antibacterial properties. Conventional strategies often rely on the sustained release of bactericidal agents, such as silver ions, which disrupt the bacterial wall and generate reactive oxygen species—mechanisms that are difficult for bacteria to overcome. However, achieving a consistent, long-term release profile is challenging, leaving the device unprotected once the agent is depleted.

To circumvent these limitations, a new frontier in surface science focuses on topographical engineering to prevent initial bacterial interaction. Micro- and nanostructured, low-adhesion, and super-hydrophobic surfaces have shown promise in physically modulating bacterial growth. Crucially, an ideal bacteriophobic surface must also be super-hydrophobic; otherwise, even dead bacterial matter adhering to a bactericidal coating can mask the release of active agents, negating their effect prematurely.

Therefore, next-generation antimicrobial surfaces are being designed around synergistic mechanisms: 1) employing physical impediments inherent in bacteriophobic nanostructures to limit initial attachment, and 2)

integrating a bactericidal or bacteriostatic environment via controlled release of antimicrobial substances. This dual strategy promises superior effectiveness, prolonged duration, and broad-spectrum applicability against various bacterial strains, making it a highly promising avenue for next-generation medical material development." This investigation aimed to establish a direct correlation between controlled surface topographical modifications at the micro/nano scale and the resulting differences in bacterial adhesion. We utilized plasma-polymerized penta-fluorophenyl methacrylate (pp-PFM) thin films, deposited on flexible silicone substrates, as a scaffolding layer to anchor metallic silver via the Tollens' reaction. By precisely modulating the plasma polymerization parameters, we achieved fine-grained control over the resulting roughness and thickness of the silver nanostructure layer. Three distinct silver surface morphologies were fully characterized using Field Emission Scanning Electron Microscopy (FE-SEM) to visualize structure. To elucidate the requirements for achieving a successful 'bacteriophobic effect,' additional surface properties were quantified, including wettability (Water Contact Angle, WCA), silver content (Inductively Coupled Plasma, ICP analysis), and protein adsorption capacity (Micro-BCA assay). The anti-adhesion performance was evaluated against a panel of relevant pathogens, encompassing both Gram-negative species (Pseudomonas aeruginosa and E. coli) and the Gram-positive bacterium, S. aureus. A multi-faceted analytical approach was employed to dissect the interaction mechanisms: FE-SEM provided high-resolution insight into the physical immobilization patterns of bacteria on each surface, while Confocal Microscopy with live/dead staining differentiated between surfaces that physically repelled bacteria (bacteriophobic) and those that actively killed them (bactericidal). Quantitatively, the efficacy was confirmed by direct bacterial counts, demonstrating significant reductions in adhesion relative to the uncoated elastomeric substrate.

Materials and Methods

Materials

The various chemical constituents and substrates necessary for fabricating and testing the surfaces were obtained from five distinct commercial sources. Silicon wafers, serving as the base platform, were procured from Wafer World in West Palm Beach, FL, USA. The plasma-polymerized films were generated using PFM monomer purchased from Apollo Scientific Ltd. (Stockport, U.K.). A comprehensive selection of analytical and treatment agents, including silver nitrate, SDS, nitric acid, Hellmanex, and D-(+)-Glucosamine hydrochloride, were consolidated from Sigma-Aldrich. For device encapsulation, the Sylgard 184 kit was supplied by Ellsworth Adhesives (Madrid, Spain), while the necessary solvent, ethanol, was provided by Scharlab (Barcelona, Spain)."

Methods

PDMS coupons were prepared following established protocols within our laboratory [1]. Sylgard 184 kit (10:1 ratio) from Ellsworth Adhesives (Spain) was utilized, with the liquid mixture applied onto flat glass using a paint applicator to establish a consistent film thickness of 500 µm500\ \mu\text{m}500 µm. These films were subsequently cured by overnight incubation at 60 ∘C60\ ^\circ\text{C}60 ∘C. The cured material was then sectioned into uniform 10 mm10\ \text{mm}10 mm diameter circular coupons. Prior to use, the coupons underwent rigorous cleaning: immersion in a 5%5\%5% SDS solution, followed by two rinses with Milli-Q water, and a final preservation rinse in 70%70\%70% ethanol. Immediately before any experimental procedure, the ethanol was removed and the coupons were thoroughly dried using an air hose."

Plasma processing

Plasma reactor

Surface modification was achieved using a vertical plate plasma reactor (GEMAT group, Barcelona, Spain) [1, 2], comprising a stainless-steel chamber acting as the ground electrode and an aluminum RF electrode for sample placement. Monomer (PFM) and process gases (argon and oxygen) were carefully metered into the system via a manifold regulated by a network of needle valves. The operating conditions were strictly controlled: a standard base pressure of 6×10−4 mbar6 \times 10^{-4}\ \text{mbar}6×10−4 mbar was established across all experiments. The PFM monomer vapor was subsequently introduced at a controlled, constant partial pressure between 0.020.020.02 and 0.04 mbar0.04\ \text{mbar}0.04 mbar to facilitate polymerization onto the supported substrates.

Plasma polymerization

The primary substrates for this study were PDMS coupons, which were subsequently coated with plasma-polymerized penta-fluorophenyl methacrylate (pp-PFM) en route to final silver coating. To ensure polymerization consistency, control experiments were also conducted on bare silicon wafers. The plasma polymerization technique employed was consistent with that previously reported [2]. Both the PDMS coupons and a silicon wafer were positioned centrally on the aluminum RF electrode within the reactor. To prevent contamination, the chamber underwent an initial cleaning phase, subjected to a 1-hour1\text{-hour}1-hour continuous wave O2/Ar\text{O}_2/\text{Ar}O2/Ar plasma (1:1 ratio) at 150 W150\ \text{W}150 W. The actual polymer deposition was a two-stage process: Initially, PFM monomer vapor was introduced. Once the monomer flow stabilized, a continuous RF power of 15 W15\ \text{W}15 W was applied, initiating a pulsed plasma polymerization sequence (10 s10\ \text{s}10 s on/10 s10\ \text{s}10 s off) for a duration optimized to achieve the target thickness and morphological characteristics (tortuosity\text{tortuosity}tortuosity) of the pp-PFM films **(Table 1).** Following the deposition phase, the plasma discharge was halted while the PFM vapor flow continued for a defined post-polymerization period. Once complete, the pp-PFM samples were retrieved from the chamber and stored under an inert argon atmosphere until needed.

Table 1. Plasma polymerization conditions for pp-PFM PDMS modification to obtain specific metallic silver structures.

	Polymerization time/min	**Post-polymerization time/min**
A–Sharp Blades	3	3
B–Thick Blades	3	10
C–Leaves	10	10

Silver immobilization

Following the deposition of the pp-PFM thin film onto the PDMS substrates, the surfaces were functionalized to anchor the subsequent silver layer. This involved incubating the samples in a 1 M1\ \text{M}1 M glucosamine solution, adjusted to pH 7.4\text{pH}\ 7.4pH 7.4, for a minimum of 6 hours6\ \text{hours}6 hours. This prolonged incubation ensured the reaction between the surface-bound pentafluorophenyl groups and the glucosamine, thereby immobilizing the sugar moieties onto the polymer chains. After incubation, samples were rinsed thoroughly with Milli-Q water and dried under an argon atmosphere. The metallic silver coating was then achieved via the reduction of silver ions using a modified Tollens' reaction. The preparation of the active Tollens' reagent commenced with the addition of 100 µL100\ \mu\text{L}100 µL of 1 M NaOH1\ \text{M}\ \text{NaOH}1 M NaOH to 1 mL1\ \text{mL}1 mL of 0.1 M silver nitrate0.1\ \text{M}\ \text{silver nitrate}0.1 M silver nitrate, which immediately resulted in silver oxide precipitation. Subsequent addition of 100 µL100\ \mu\text{L}100 µL of 30%30\%30% ammonia led to the complete dissolution of the precipitate, forming the required diamminesilver(I) complex. The glucosamine-modified coupons were then immersed in 4 mL4\ \text{mL}4 mL of this fresh Tollens' reagent per vial and heated in a water bath at 90 ∘C90\ ^\circ\text{C}90 ∘C for the required reaction duration to reduce the silver ions to metallic silver upon contact with the surface-bound glucosamine.

Surface characterization

The properties of the silver-modified surfaces were assessed using several analytical techniques. Surface hydrophobicity was quantified by measuring the water contact angle (WCA) using a DSA100 tensiometer (Krüss). Surface morphology was examined via Field Emission Scanning Electron Microscopy (FE-SEM, Merlin) operating at 15 kV15\ \text{kV}15 kV. Notably, no gold sputtering was applied to these samples to maintain the integrity of the underlying surface chemistry while ensuring sufficient conductivity for imaging. Surface roughness parameters were rigorously quantified by analyzing over 50 SEM50\ \text{SEM}50 SEM micrographs using ImageJ software (http://www.imagej.nih.gov/) with the SurfCharJ plug-in, adhering to the standards defined by ISO 4287/2000 [3] for local roughness analysis. The total silver loading and any subsequent silver leaching from the surfaces were precisely determined using Inductively Coupled Plasma Optical Emission Spectroscopy (ICP-OES Optima 2100 DV2100\ \text{DV}2100 DV, PerkinElmer). For this analysis, silver samples were first digested in 30%30\%30% nitric acid and then diluted 1:1001:1001:100 in Milli-Q water. Finally, protein adhesion studies were conducted by adapting the protocol established by Hohmann *et al.* [4]. Fetal-bovine serum (FBS\text{FBS}FBS) served as the complex-protein medium. After 24 hours24\ \text{hours}24 hours of

incubation, samples were washed twice with isopropanol, followed by the addition of RIPA\text{RIPA}RIPA buffer (Sigma-Aldrich®, Germany). Following a 30 -minute30\ \text{-minute}30 -minute incubation at 37 ∘C37\ ^\circ\text{C}37 ∘C in the buffer, the quantity of adsorbed protein was quantified using the Micro BCATM\text{BCA}^{\text{TM}}BCATM Protein Assay Kit (Thermo Fisher Scientific®, Spain), with bovine serum albumin (BSA\text{BSA}BSA) used as the standard reference."

Assessment of bacteriophobic properties

The bacterial strains for this study were sourced from ATCC®, The Global Bioresource Center in the USA. The strains included: 1) Pseudomonas aeruginosa PA01 (ATCC 15692™), a gram-negative opportunistic pathogen commonly used in research, featuring a single unsheathed polar flagellum that contributes to both its motility and virulence, including adhesion; 2) Escherichia coli CFT073 (ATCC 700928™), a gram-negative uropathogenic strain isolated clinically, possessing multiple fimbriae with specific adhesins as identified in its genome sequence [5]; and 3) Staphylococcus aureus subsp. aureus (ATCC 33592™), a gram-positive strain resistant to gentamicin and methicillin. All strains are handled under biosafety level 2 conditions. These bacteria were selected as models for biofilm formation, multi-drug resistance, and fimbriae-mediated attachment, and they are frequently associated with hospital-acquired infections. To prepare the inoculum, a single colony from each strain was grown in 50 mL of the suitable growth medium—LB broth for E. coli CFT073, and TSB for P. aeruginosa PA01 and S. aureus—and incubated at 37 °C with agitation overnight.

Bacterial viability

To evaluate bacterial growth on PDMS versus the coated surfaces, optical density (OD) at 600 nm was recorded using a spectrophotometer (Spectramax M2, Molecular Devices, USA) over a period of 18 to 50 hours at 37 °C. Additionally, the Minimum Bactericidal Concentration (MBC) was determined for all three bacterial strains used in this study.

Bacterial adhesion

To study bacterial attachment, the initial cultures were diluted in fresh media and grown until the optical density at 600 nm reached 0.02. Bacteria were then applied to PDMS coupons (control) and to the experimental coated surfaces, and incubated under static conditions at 37 °C for roughly 20 hours. The extraction method was based on Mandakhalikar *et al*. [6].

After incubation, samples were gently rinsed twice with sterile PBS at room temperature to remove loosely bound bacteria. Each coupon was then transferred to a sterile tube containing 2 mL of PBS, sonicated for 10 minutes at 70 Hz, vortexed for 2 minutes, and sonicated again for another 10 minutes to detach adherent cells. Empty coupons were discarded. The recovered bacterial suspension was centrifuged at 4,500 × g for 20 minutes, washed twice with PBS, and resuspended for serial dilution.

Diluted samples were plated onto media specific for each strain: LB-agar for E. coli CFT073, and TSA (TSB-agar) for P. aeruginosa PA01 and S. aureus subsp. aureus. Plates were incubated at 37 °C for 18–36 hours depending on the strain, and colony-forming units (CFUs) were counted to quantify surface-adhered bacteria.

Statistical analysis

Each surface adhesion assay was repeated three times, with four independent replicates per trial (n = 4). Once bacterial attachment was measured, the data were analyzed using one-way ANOVA followed by multiple comparison tests. PDMS served as the reference control to evaluate differences in adhesion. Statistical significance was determined based on p-values, with thresholds defined as: $P > 0.05$ (not significant, ns), $P < 0.05$ (), $P < 0.01$ (), and $P < 0.001$ (). All analyses were carried out using GraphPad Prism software.

Bacterial visualization

For FE-SEM observations, an initial culture of E. coli CFT073 was diluted in fresh media and grown until reaching an optical density (OD_{600}) of 0.02. The bacteria were then applied to the surface coupons and incubated under static conditions at 37 °C overnight. After incubation, samples were rinsed twice with sterile PBS at room temperature to remove non-adherent cells. The attached bacteria were fixed with 4% formaldehyde for a minimum of 2 hours at room temperature. Following fixation, formaldehyde was removed by washing with PBS, and the samples underwent graded dehydration using ethanol solutions at 30%, 50%, and 70% for 30 minutes each,

finishing with a 90% ethanol wash. The surfaces were then sputter-coated with gold prior to FE-SEM imaging. For confocal microscopy, surfaces exposed to bacteria were prepared using the LIVE/DEAD™ BacLight™ Bacterial Viability Kit (L7007, ThermoFisher®, USA) according to the manufacturer's instructions, allowing visualization of live and dead bacterial cells.

Results and Discussion

Preparation of pp-PFM/silver coating and characterization

Our research group has previously investigated the antibacterial properties of metallic silver coatings immobilized on flexible substrates using plasma-polymerized pentafluorophenyl methacrylate (pp-PFM) as a release platform. Thin films of pp-PFM serve as a reactive coating due to the presence of ester groups, which can form covalent bonds with molecules containing amine functionalities [2, 7, 8]. By incubating pp-PFM films with D-(+)-Glucosamine hydrochloride, the sugar was covalently attached to the polymer backbone, creating a reductive surface capable of generating nanostructured metallic silver via Tollens' reaction. The resulting silver nanostructures were confirmed to be metallic using EDX, in agreement with previous reports [2]. In this system, the controlled release of silver ions through local surface oxidation enhanced bacterial killing and partially inhibited bacterial adhesion and colonization [9]. In the present study, we demonstrated that the plasma polymerization conditions **(Table 1)** can be tuned to adjust the thickness and tortuosity of the pp-PFM films, which in turn influenced the morphology and nanostructure of the immobilized silver layer. Three distinct nanostructures were observed on the silver-coated surfaces: "sharp blades," "thick blades," and "leaves" **(Figure 1).** Among the factors affecting PFM polymerization, polymerization time (duration of PDMS exposure to pp-PFM plasma) and post-polymerization time (duration the pp-PFM vapor was maintained after polymerization) were the most critical in determining the final nanostructure.

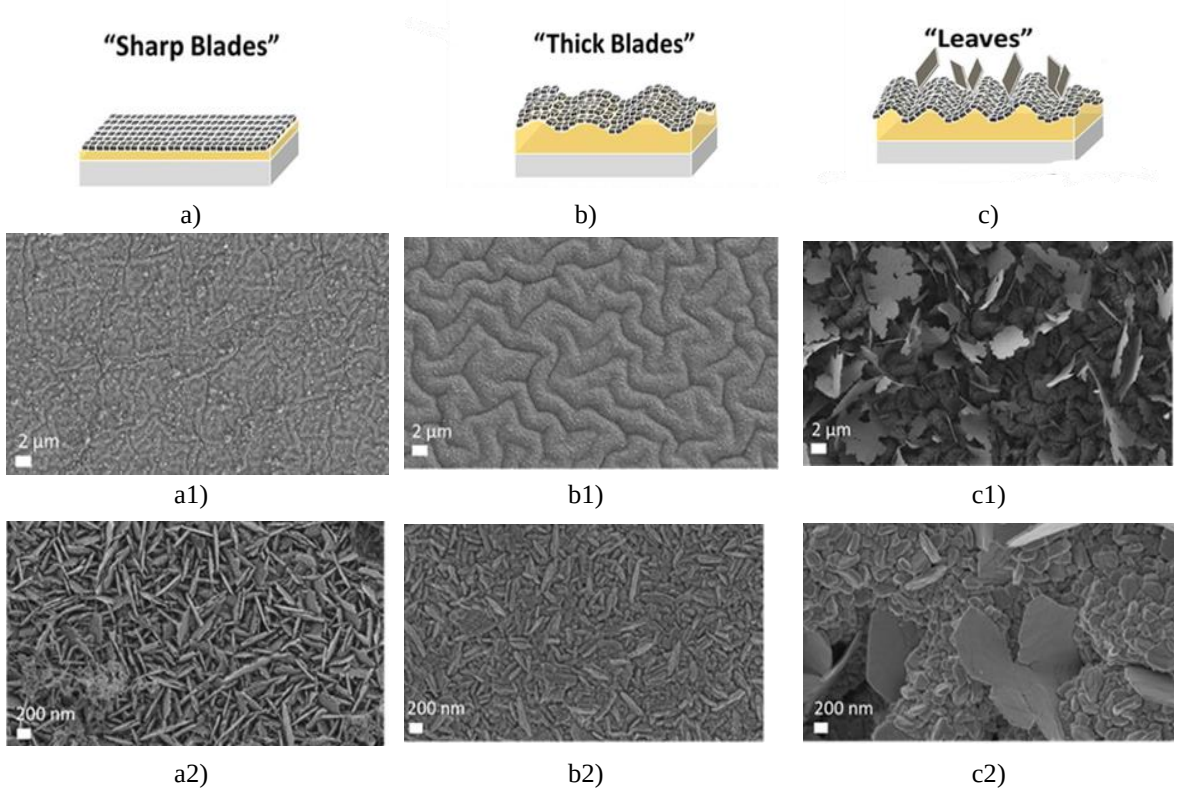

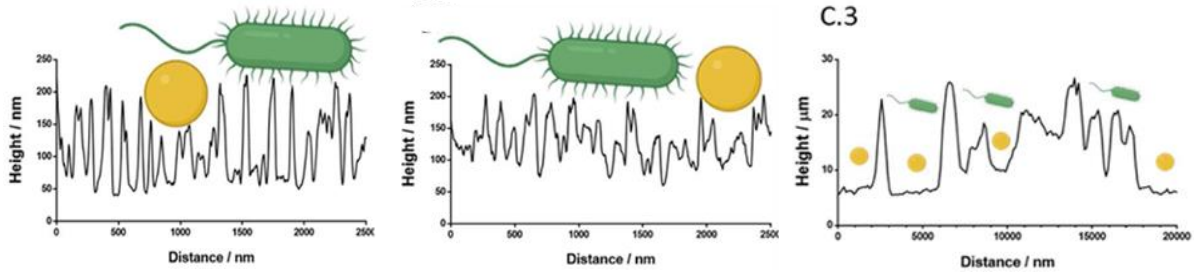

a3) b3) c3)

Figure 1. The field emission scanning electron microscopy (FE-SEM) images illustrating three types of silver-coated surfaces.

The accompanying graph shows the base PDMS substrate (dark grey), the pp-PFM layer (yellow) exhibiting distinct morphologies corresponding to its tortuosity, and the silver coating with different nanostructures (light grey). The surfaces were categorized based on the pp-PFM tortuosity and the morphology of the silver layer: "sharp blades" (a, a1, a2), "thick blades" (b, b1, b2), and "leaves" (c, c1, c2). The impact of surface morphology on bacterial adhesion was inferred from roughness profiles of the sharp blades (a3), thick blades (b3), and leaves (c3), with a schematic representation of bacterial size included for scale. Short polymerization and post-polymerization times (3 minutes each) produced thin pp-PFM films where silver nucleation generated fine, sharp nanostructures approximately 200 nm long and a few nanometers wide, designated as "sharp blades" **(Figures 1a1 and 1a2).** Extending the post-polymerization period allowed further PFM chain termination and reaction with residual vapor, creating a "mountainous" topography with more pronounced peaks and valleys measuring 2–4 µm **(Figure 1b1).** Silver deposition on these surfaces produced wider blades, termed "thick blades" **(Figure 1b2)**. Longer polymerization and post-polymerization times (10 minutes) increased chain tortuosity, resulting in complex structures. Silver nucleation on these films produced the "leaves" morphology, consisting of slender nanosheets under 50 nm thick covering the main surface **(Figure 1c1).** Beneath these leaves, the underlying mountainous topography persisted, accompanied by larger nanoparticles exceeding 200 nm **(Figure 1c2).** Surface roughness profiles were analyzed to understand how these morphologies could hinder bacterial adhesion and provide insight into the bacteriophobic mechanism. For the sharp blades, the profile indicated blade heights of ~150 nm spaced less than 100 nm apart **(Figure 1a3)**, while thick blades showed similar features with heights around 100 nm and spacing under 80 nm **(Figure 1a3).** These nanoscale features are believed to physically limit bacterial interaction and attachment [10]. Schematics illustrate how multiscale wrinkled surfaces reduce the contact area available to bacteria, impeding colonization. The leaves structure presents a more complex topography due to its amorphous, nanosheet-like morphology. Individual leaves reach up to 10 µm in height, less than 50 nm in thickness, and can be separated by more than 2 µm **(Figure 1a3)**. The larger spacing initially allows bacteria to interact with the surface; however, the fine nanostructures of the leaves likely influence adhesion once contact occurs. Surface hydrophobicity was also evaluated because it affects bacterial attachment. Rough surfaces with lower hydrophobicity generally provide more sites for bacterial colonization, protecting bacteria from shear forces in fluid environments [11-13]. Water contact angle (WCA) measurements showed that uncoated PDMS had a WCA of ~95°, consistent with typical hydrophobic silicone behavior. In contrast, all modified silver-coated surfaces exhibited WCAs around 150°, indicating superhydrophobic properties **(Figure 2a)**.

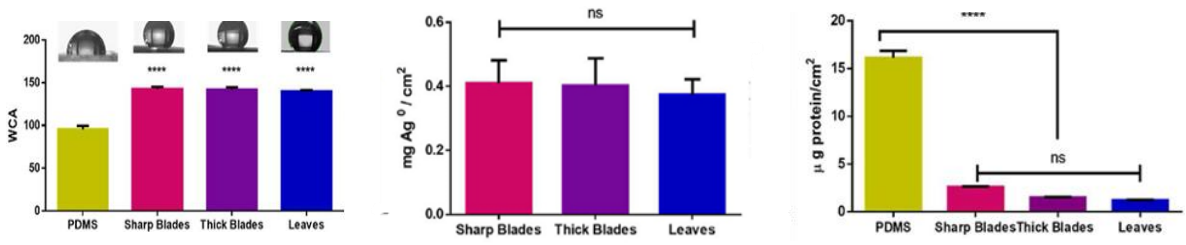

a) b) c)

Figure 2. Water contact angle (WCA) measurements of the silver-coated surfaces compared to uncoated PDMS are shown in Figure 2a, while Figure 2b presents the quantification of silver per cm² on each surface using ICP. Figure 2c depicts the amount of protein adsorbed per cm² after 24 hours of incubation with Fetal

Bovine Serum (FBS). Statistical analysis revealed significant differences between the control and all three silver-coated surfaces, with p-values ranging from <0.05 () to <0.001 (*). The nanoscale structuring of the silver surfaces generates pronounced roughness, which enhances hydrophobicity to a superhydrophobic range. According to previous studies, the combination of nanoscale roughness and superhydrophobic behavior can reduce bacterial adhesion by acting as an antifouling surface and trapping air beneath the liquid layer, producing a bacteriophobic effect [11, 14–16]. Next, the total silver content on the surfaces was assessed. Interestingly, all surfaces contained comparable amounts of silver (Figure 2b), regardless of their structural complexity. This suggests that the observed superhydrophobicity is not due to an increased amount of silver, but rather to the way silver is distributed and anchored on the surface. Therefore, differences in bacterial adhesion are attributed primarily to the nanoscale structuring of the silver layer. Protein adsorption studies with FBS showed that pp-PFM-silver coated surfaces significantly reduced protein deposition compared to uncoated PDMS (Figure 2c). Since protein adsorption can facilitate bacterial attachment, these surfaces not only create a physical barrier to adhesion but also limit protein-mediated bacterial interactions [17, 18]. This combination of nanoscale topography and reduced protein binding is expected to provide a durable bacteriophobic effect. As highlighted in the literature [19], polymer CVD methods are compatible with a wide range of substrates, including delicate or elastic materials, as well as complex geometries such as sensors, particles, or microtrenches [2, 20, 21]. This indicates that recreating these nanostructured surfaces on medical devices could be achieved with minimal process modifications.

Silver ions release and its effect on bacterial growth

The release of silver ions from the coated surfaces plays a key role in both bacterial adhesion and the bacteriostatic or bactericidal activity of the material [22, 23]. Measuring the amount of silver released into the surrounding medium provides insight into the relative contribution of silver ions versus surface nanostructure in controlling bacterial attachment; lower silver ion concentrations suggest that the nanoscale surface features are primarily responsible for reducing adhesion. Following the Tollens' reaction, the surfaces consisted of a continuous metallic silver layer, in contrast to antibacterial coatings formed from aggregated silver nanoparticles, which typically release higher amounts of colloidal silver. To quantify the cumulative release of silver ions from the three engineered silver surfaces, 1 mL of medium was collected at various time points over 530 hours (and replaced with fresh medium) and analyzed by ICP **(Figure 3a).** To ensure that the detected silver ions were not merely due to chemo-adsorbed silver from the Tollens' reaction, additional release profiles were obtained by immersing the samples in acetic acid.

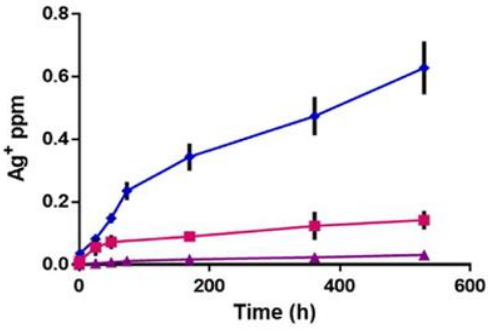

a)

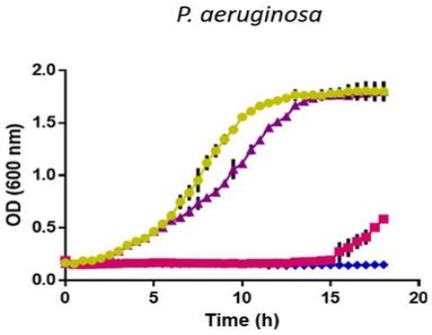

b)

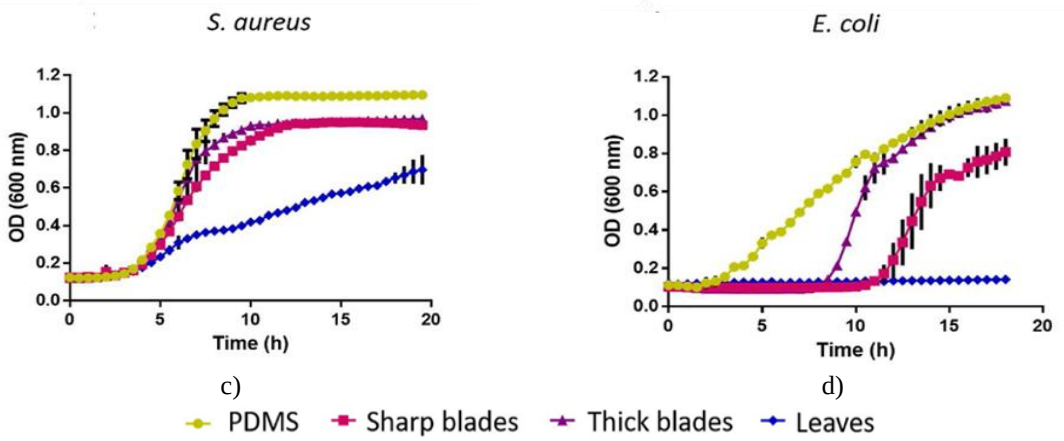

Figure 3. illustrates the cumulative release of silver ions from the nanostructured surfaces (a) and the growth curves of Pseudomonas aeruginosa PAO1 (b), Staphylococcus aureus subsp. aureus (c), and Escherichia coli CFT073 (d) in contact with PDMS as a control and the three silver surfaces ("sharp blades," "thick blades," and "leaves").

The three silver surfaces exhibited distinct ion release profiles due to differences in their nanostructure. The "leaves" morphology showed an initial burst of 0.23 ± 0.03 ppm within the first 72 hours, followed by a slower, sustained release **(Figure 3a)**. This pattern is likely caused by local oxidation of the thin, high-surface-area leaves when exposed to oxygen in the bacterial medium. The early release corresponds to the oxidation of thinner leaves, while the subsequent slower release involves thicker leaves. Even after 530 hours (22 days), the release had not plateaued, indicating that the leaves act as a significant silver reservoir.

In contrast, the "sharp blades" surface exhibited a minimal initial burst of 0.05 ± 0.02 ppm during the first 24 hours, followed by a sustained release approaching a plateau. The limited exposure of the sharp blades to the medium reduces local oxidation, explaining the slower, steadier ion release. The "thick blades" morphology released the lowest amount of silver, close to the detection limit (10 ppb), likely due to increased blade thickness and tortuosity, which stabilizes the silver layer and protects it from oxidation. These results suggest that the "thick blades" structure contributes negligibly to silver ion release.

To assess the effect of these different release profiles, the silver surfaces were incubated with three bacterial strains: P. aeruginosa PAO1, S. aureus subsp. aureus, and E. coli CFT073 **(Figures 3b–3d)**. Bacterial growth correlated with the observed silver release. Surfaces with the "leaves" morphology displayed a pronounced bacteriostatic effect on gram-negative strains, completely inhibiting growth of P. aeruginosa and E. coli, while only delaying growth in the gram-positive S. aureus. Extending the growth curves to 50 hours confirmed that gram-negative strains did not grow, and gram-positive bacteria did not reach the stationary phase.

To further differentiate bacteriostatic versus bactericidal effects, samples from the "leaves" surface after 18 hours were transferred to fresh medium and monitored overnight. Erratic growth in E. coli and P. aeruginosa indicated that the bacteria were alive but replication was inhibited, consistent with a bacteriostatic effect. For S. aureus, very low absorbance values suggested a substantial reduction in bacterial population, though not complete elimination. This partial resistance aligns with the known structure of gram-positive cell walls, which contain multiple peptidoglycan layers (15–80 nm thick) that hinder silver ions from effectively interacting with internal components such as the respiratory chain or secretion systems [22, 24, 25]. Consequently, while silver ions reduce bacterial proliferation, surfaces cannot be considered fully bactericidal against gram-positive strains.

In contrast, the silver ions released from the "sharp blades" surface exhibited a different profile compared to the "leaves" morphology, showing an overall lower release. This resulted in a brief delay at the onset of the exponential growth phase for all bacterial strains **(Figures 3b–3d)**, which corresponds to the initial burst of silver ions **(Figure 3a)**. This early release temporarily inhibited bacterial replication but was insufficient to fully prevent growth. Once bacteria reached a critical population, they overcame the inhibitory effect of silver ions and entered their normal exponential phase. This effect was less pronounced for S. aureus **(Figure 3c)**. Extended incubation up to 50 hours for P. aeruginosa and E. coli showed that the growth curves eventually reached the stationary phase, closely resembling the PDMS control. These observations indicate that the silver ion release slows bacterial growth without killing the cells.

For the "thick blades" surfaces, silver ion release had no detectable impact on bacterial growth for any of the strains tested **(Figure 3).** A slight extension of the adaptation phase was observed for E. coli, but the stationary phase was reached at the same time as the control after 18 hours, indicating typical growth. This is consistent with the silver release data **(Figure 3a)**, where negligible amounts of ions were detected. Consequently, any differences in bacterial adhesion on this surface can be attributed solely to surface morphology rather than silver ion effects.
To further confirm that bacteria were inhibited rather than killed, minimum bactericidal concentration (MBC) tests were performed using silver. These results, combined with the cumulative silver release over 22 days **(Figure 3a),** indicate that the released silver was insufficient to fully eliminate bacterial populations.
From a cytotoxicity perspective, the daily silver release from "sharp blades," "thick blades," and "leaves" surfaces remains well below levels of concern. The maximum daily release did not exceed 0.1 ppm **(Figure 3a)**, which aligns with the World Health Organization's guideline for safe silver consumption in water (WHO/HEP/ECH/WSH/2021.7). While limited data exist regarding skin exposure to silver, no cases of argyria have been reported from the use of lotions or medical devices containing high silver concentrations. The Agency for Toxic Substances and Disease Registry permits up to 81 ppm/day of silver in contact with skin (Silver CAS#7440-22-4). Therefore, all the tested surfaces, including the "leaves" morphology, could be safely applied to implantable devices or materials in close contact with human skin.

Bacteriophobic effect characterization

To investigate the impact of the nanostructured silver surfaces on bacterial adhesion, samples were analyzed using FE-SEM, live/dead staining, and bacterial quantification, employing the same strains evaluated in **Figure 3**.
Initially, bacterial attachment was examined via FE-SEM. E. coli (Gram-negative) and S. aureus (Gram-positive) were chosen as representative strains due to their relevance as clinical pathogens and the presence of specialized appendages that mediate interactions with tissues and surfaces [26, 27]. Unmodified PDMS served as the control **(Figure 4a),** showing a uniform, multilayered bacterial coverage, indicating that the surface allowed bacterial adhesion without obstruction. On PDMS, E. coli were randomly distributed, suggesting that the native topography of the silicone did not influence orientation or preferential attachment. Actively dividing cells were observed, demonstrating that bacteria remained metabolically active on PDMS. No evidence of selective colonization, such as clustering in particular areas, orientation bias, or morphological deformation, was detected on the control surface.

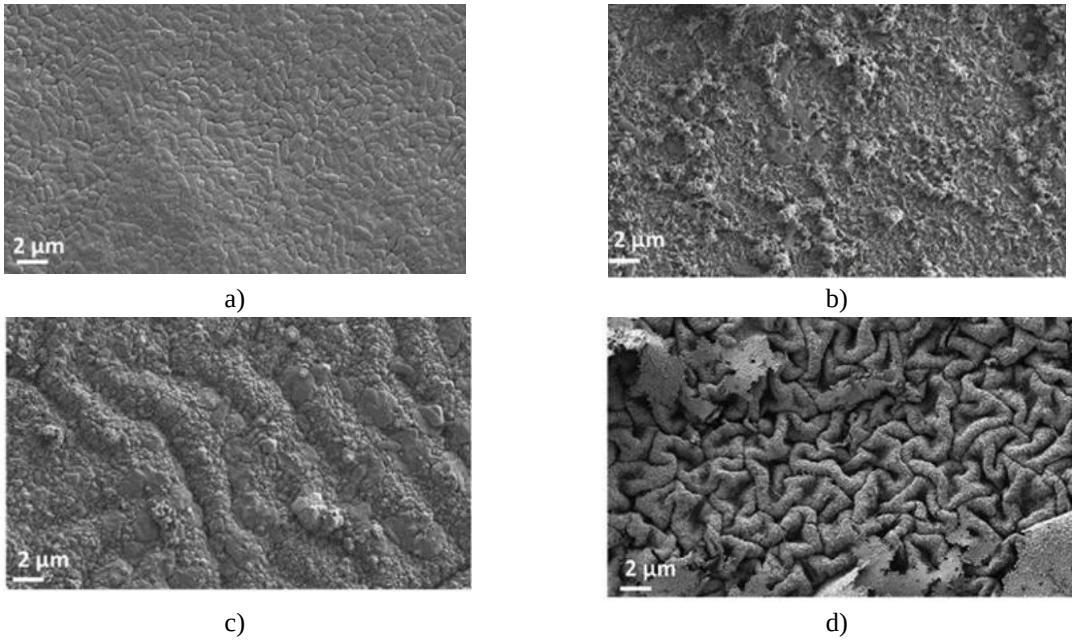

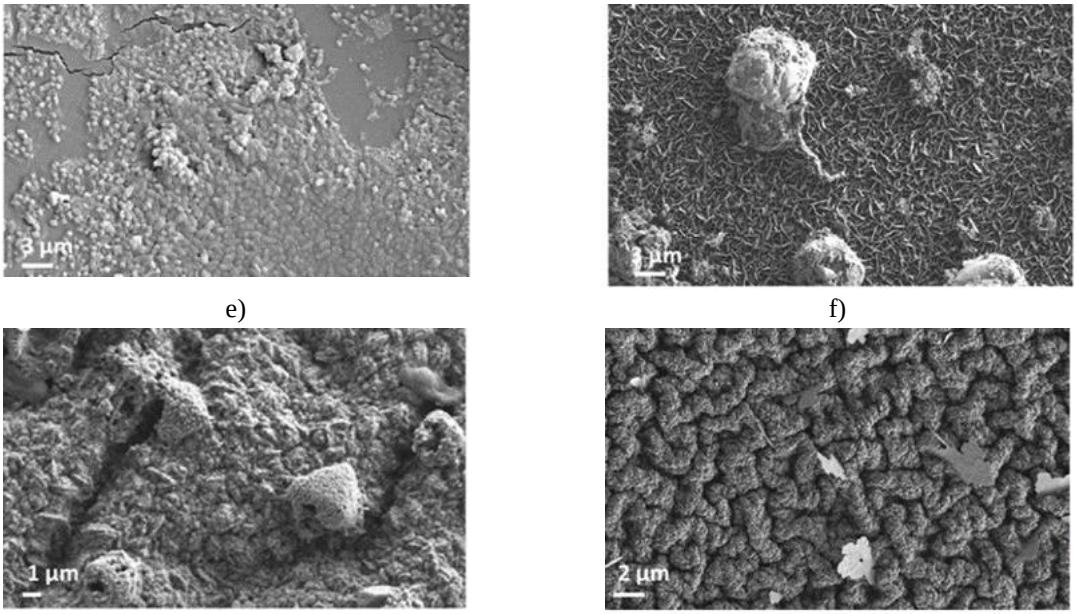

Figure 4. FE-SEM Analysis of Bacterial Adhesion on Silver-Coated Surfaces
Field emission scanning electron microscopy (FE-SEM) images show PDMS as the control surface (a, e), and the silver-coated surfaces with "sharp blades" (b, f), "thick blades" (c, g), and "leaves" (d, h) after incubation with E.
coli CFT073 (upper panels) and S. aureus (lower panels). For visualization purposes, E. coli were artificially colored green.

Compared with PDMS, the "sharp blades" surface **(Figure 4b)** exhibited a marked reduction in bacterial attachment. Cells were randomly distributed without preferred orientation. The sharp blade topography appears to physically disrupt bacterial membranes, contributing to bacterial elimination—a mechanism consistent with previously reported physical antimicrobial surfaces [28, 29]. No bacterial aggregates or microcolonies were observed, suggesting that the few adhered cells represent random attachment. This effect likely arises from a combination of the nanoscale roughness **(Figure 1a3)**, blade morphology capable of mechanically damaging membranes, and the superhydrophobic surface properties **(Figure 2a).**

The "thick blades" surface **(Figure 4c)** showed a different behavior: bacteria tended to align within the grooves of the surface rather than on the raised regions. No structural membrane damage was observed, and overall bacterial coverage was low, similar to the "sharp blades" surface. Because this surface did not release silver ions, the reduced adhesion can be attributed primarily to the combined effects of surface morphology and superhydrophobicity **(Figures 1b3 and 2a).** Weak interactions between bacteria and the surface prevent stable attachment, allowing cells to be easily removed from the surface and limiting biofilm formation. FE-SEM images also indicated minimal adhesion of S. aureus on both "thick blades" and "sharp blades" surfaces, with only small amounts of precipitates, cell debris, or spherical aggregates visible **(Figures 4f and g)**, highlighting the potential of these morphologies to reduce Gram-positive bacterial colonization.

In contrast, the "leaves" surface **(Figure 4d)** exhibited significant structural changes after bacterial incubation. Many leaf-like structures detached, leaving behind eroded areas and revealing the underlying "mountainous" topography with more pronounced grooves than other silver surfaces. These leaves appear to be loosely anchored extensions of the nano-blade structures present on other surfaces, creating a dynamic layer that actively releases silver ions into the medium. This extensive ion release correlates with the observed aberrant bacterial growth or complete inhibition across all strains, as previously shown in the growth curves **(Figure 3)**. Similar behavior was seen for S. aureus on the "leaves" surface **(Figure 4h)**, with only a few bacteria adhering randomly and spherical precipitates dominating the surface.

Due to the structural changes induced by exposure to the medium, FE-SEM alone cannot fully reveal bacterial interactions with the "leaves" morphology. However, confocal microscopy, which allows distinction between live

and dead cells, provides a clearer picture of bacterial responses to the detachment and ion release of silver leaves **(Figure 5)**.

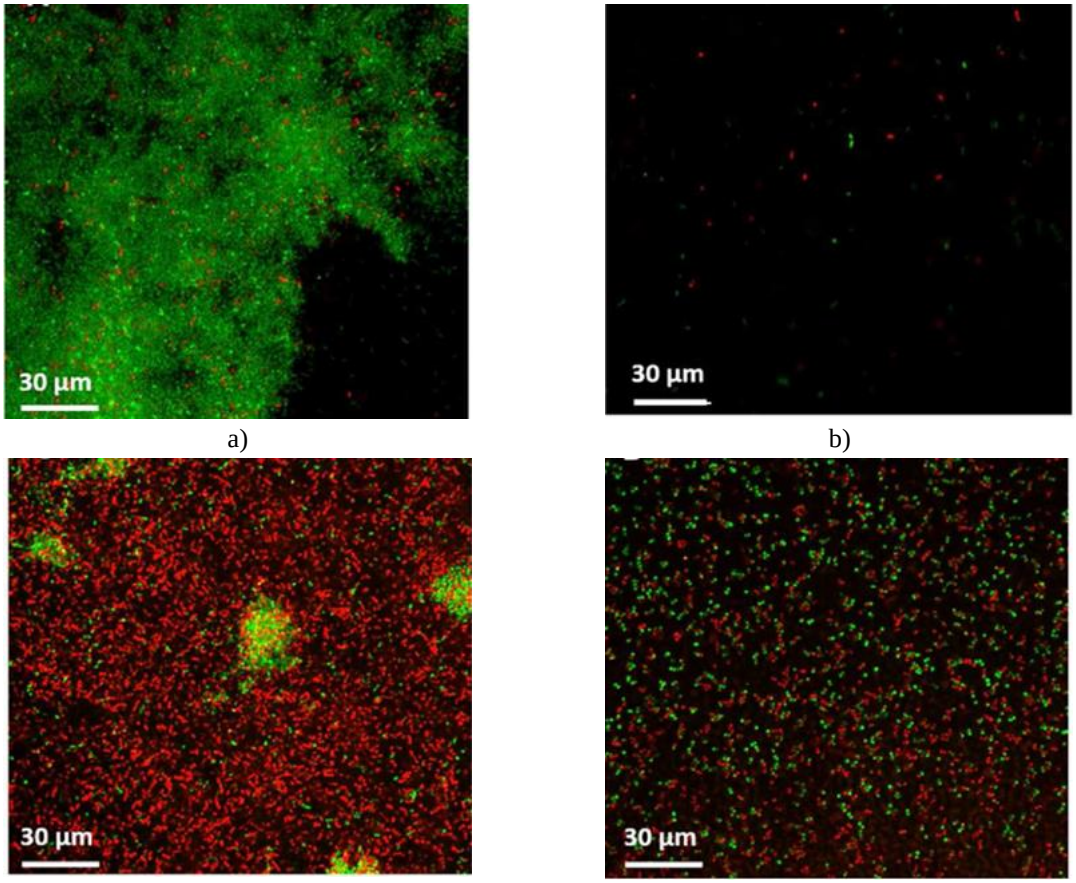

Figure 5. Confocal Microscopy of Bacterial Adhesion and Viability
Confocal microscopy images show PDMS incubated with P. aeruginosa (a) and silver "leaves" surfaces incubated with E. coli (b), S. aureus (c), and P. aeruginosa (d). Samples were stained using a Live/Dead kit, where green fluorescence indicates live, metabolically active bacteria, and red fluorescence marks dead bacteria with compromised membranes. The biofilm matrix itself was not stained.

To assess bacterial behavior around the "leaves" surfaces, uncoated PDMS served as the control, with P. aeruginosa representing a reference strain for attachment studies **(Figure 5a)**. On PDMS, bacteria formed a stratified, layered biofilm dominated by live cells (green), showing extensive attachment. Following adhesion, bacteria began dividing and secreting extracellular matrix, forming microcolonies that serve as precursors for structured biofilm development.

In contrast, the silver "leaves" surfaces exhibited markedly different bacterial interactions. For E. coli and P. aeruginosa, although bacterial growth in the medium was similar to what was previously observed **(Figure 3)**, adhesion to the silver "leaves" surface was drastically reduced. **Figure 5b** shows almost no E. coli attached, despite the strain possessing abundant pili and specialized adhesion structures. The combination of local silver ion release, nanoscale roughness **(Figure 1c3),** and superhydrophobicity **(Figure 2)** appears to create a bacteriophobic effect that prevents stable bacterial attachment.

P. aeruginosa **(Figure 5c)** did attach to the surface in notable numbers; however, most attached cells were dead (red), likely due to silver ion exposure. Individual bacteria were observed without formation of biofilm, although small clusters of live cells (green) were occasionally seen among dead bacteria, suggesting that surface erosion may reduce the barrier effect over time. For S. aureus **(Figure 5d)**, bacteria adhered more extensively to the "leaves" surface, with a roughly equal mix of live and dead cells. This higher level of attachment is consistent with the reduced sensitivity of S. aureus to silver ions. Nevertheless, adhesion was localized and reversible, with individual bacteria observed and no signs of stable clusters or biofilm formation.

To quantitatively assess surface colonization, the total number of viable bacteria was measured. Surfaces were incubated with each bacterial strain for 20 hours, washed to remove loosely attached cells, and the remaining bacteria were extracted, plated, and counted as colony-forming units (CFUs). **Figure 6** presents the results for E. coli, P. aeruginosa, and S. aureus on each of the nanostructured surfaces ("sharp blades," "thick blades," and "leaves"), with uncoated PDMS and pp-PFM-coated PDMS serving as adhesion controls.

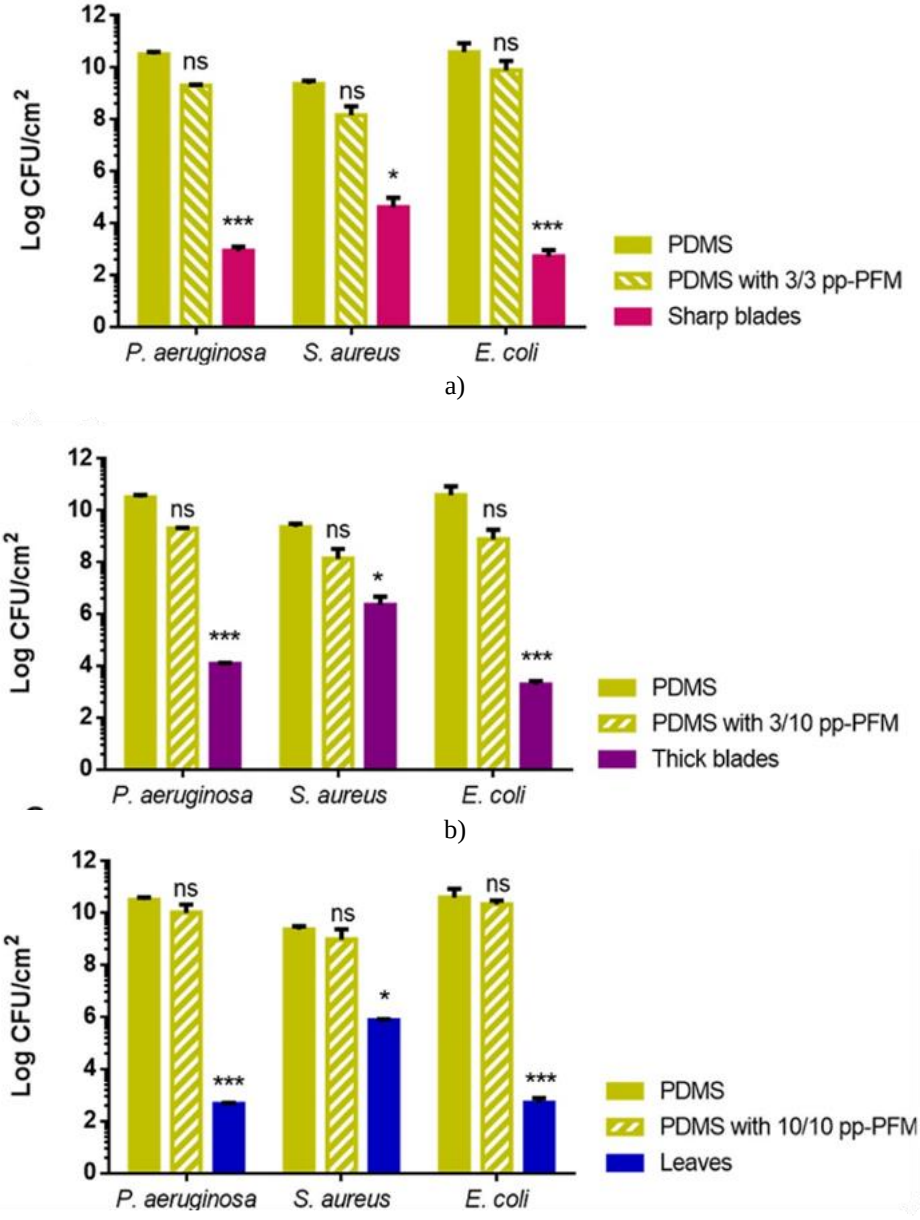

Figure 6. Quantification of Bacterial Adhesion on Silver-Coated Surfaces

Figure 6 shows bacterial adhesion (CFU/cm²) on the developed surfaces—"sharp blades" (a), "thick blades" (b), and "leaves" (c)—compared with uncoated PDMS and PDMS/pp-PFM controls (polymerized under the conditions in **Table 1**, prior to silver deposition).Three bacterial strains were tested: P. aeruginosa PAO1, S. aureus subsp. aureus, and E. coli CFT073, to confirm that the observed effects were not strain-specific. Statistical analysis indicated a significant reduction in adhesion on all silver surfaces compared to controls (p-values between <0.05 () and <0.001 (**)). Comparisons between the developed surfaces showed no significant differences (p-values ranging from 0.056 to 0.7). All three silver-coated surfaces led to a pronounced reduction in bacterial adhesion. Even in the least effective case (S. aureus on "thick blades"), adhesion decreased by at least three orders of magnitude, while the most effective case (P. aeruginosa on "leaves") showed an eight-log reduction relative to

uncoated PDMS and PDMS/pp-PFM. Despite differences in adhesion mechanisms and bacterial physiology, the overall reduction was consistently high across strains. For P. aeruginosa and E. coli, the silver surfaces were particularly effective, reducing adhesion by more than six orders of magnitude. This effect is likely due to disruption of the bacterial outer membrane, resulting from the combined action of the surface nanostructure and silver ion release, which creates an inhospitable environment at the interface. Interestingly, the "thick blades" surface **(Figure 6b)**, which does not release silver ions, achieved a comparable reduction in adhesion, demonstrating that a purely surface-based bacteriophobic effect can be as effective as a silver-ion-mediated bactericidal mechanism. Staphylococcus aureus exhibited higher adhesion overall, which can be attributed to the rigid peptidoglycan-rich cell wall characteristic of Gram-positive bacteria [30]. This structure reduces the efficacy of silver ions from the "sharp blades" and "leaves" surfaces **(Figures 6a and 6c)**, allowing more bacteria to survive in the medium and interact with the surface. Nevertheless, the "sharp blades" surface showed superior reduction of S. aureus adhesion, suggesting that the combination of surface nanostructure and silver ion release is particularly effective at disrupting Gram-positive membranes. Interestingly, the quantitative CFU counts were higher than what was observed by FE-SEM. This discrepancy likely reflects the presence of bacteria that were loosely attached and not fully anchored, emphasizing the importance of combining microscopy with colony-based assays to assess surface colonization. Overall, while all three nanostructured silver surfaces ("sharp blades," "thick blades," and "leaves") demonstrated strong bacteriophobic behavior, the underlying mechanisms of bacterial repulsion varied according to their specific nanostructure and the bacterial strain. Further investigation is needed to fully elucidate these mechanisms. Clinically, these surfaces are particularly relevant because bacteria first contact medical device surfaces during implantation [31, 32]. The results suggest that all three silver nanostructures can significantly reduce bacterial adhesion within the first 20 hours of exposure, providing a promising strategy to prevent colonization and subsequent biofilm formation.

Conclusion

In this study, we investigated metallic silver coatings immobilized on pp-PFM thin films. We found that altering the properties of the pp-PFM layer induced structural changes in the silver coating, which in turn influenced bacterial interactions and adhesion. By adjusting the polymerization conditions of pp-PFM, we identified three distinct silver morphologies, each displaying unique antibacterial behaviors: the "leaves" structure, characterized by a high specific surface area that facilitated substantial silver ion release and produced a modest bactericidal effect; the "thick blades" structure, featuring meandering nanoblades that inhibited bacterial adhesion primarily through topography-driven (bacteriophobic) effects; and the "sharp blades" structure, with finely pointed nanoblades that combined topographical effects and bacterial membrane disruption to deliver both bacteriophobic and bacteriostatic activity. All three strategies demonstrated exceptional efficacy in preventing bacterial adhesion, achieving over six orders of magnitude reduction in CFU compared to uncoated surfaces. Moreover, the versatility of these silver coatings, which can be applied to a wide range of materials including challenging elastomeric substrates, highlights their strong potential as an approach to limit bacterial colonization and biofilm formation on medical devices.

Supporting information

Schematic representation of the stainless-steel vertical plasma reactor and its electrical components. The surface modifications described in this study were carried out using a stainless-steel vertical plasma reactor manufactured by the GEMAT group (IQS-URL, Barcelona).

Fabrication of silver-based nanostructured surfaces, including the corresponding chemical reaction equations.

Energy Dispersive X-Ray (EDX) analysis of the surfaces after fabrication. Accumulative silver release in acetic acid. This test was conducted to confirm that silver release is primarily due to local surface oxidation rather than chemo-adsorbed silver.

Bacterial growth curves and endpoint measurements. Growth monitoring was extended to 50 hours to assess the long-term effects of the developed surfaces on bacterial proliferation.

Determination of the minimum bactericidal concentration (MBC) of silver for the bacterial strains tested.

FE-SEM images illustrating bacterial membrane damage.

SEM images of the pp-PFM surface prior to silver deposition.

Acknowledgments: We thank to Laboratorio de análisis de metales (IQS) and Dra. Ariadna Verdaguer to support us with the ICP analysis. The authors would like to thank to Inmaculada Luna Pineda for the edition of the manuscript.

Conflict of Interest: Tractivus is a company that work in the development of antifouling surfaces. However, Tractivus does not have any commercial interest in the results presented in this paper. The patent is related with the development of antifouling surfaces, but the paper submitted is basic science and it is not useful for strengthening the patent. Thus, the authors confirm that there are no known conflicts of interest associated with this publication and there has been no significant financial support for this work that could have influenced its outcome.

Financial Support: This work was supported by Agència de Gestió d'Ajuts Universitaris i de Recerca (SGR-1559 & 2016-DI073), and by Ministerio de Ciencia, Innovación y Universidades (RTC-2017-6668-1).

Ethics Statement: None

References

1. Texido R, Borros S. Allylamine PECVD modification of PDMS as simple method to obtain conductive flexible polypyrrole thin films. Polymers. 2019;11(12):2108.
2. Gilabert-Porres J, Martí S, Calatayud L, Ramos V, Rosell A, Borros S. Design of a nanostructured active surface against gram-positive and gram-negative bacteria through plasma activation and in situ silver reduction. ACS Appl Mater Interfaces. 2016;8(1):64-73.
3. Chinga G, Johnsen PO, Dougherty R, Berli EL. Quantification of the 3D microstructure of SC surfaces. J Microsc. 2007;227:254-65.
4. Hohmann S, Neidig A, Kühl B, Kirschhöfer F, Overhage J, Brenner-Weiß G. A new data processing routine facilitating the identification of surface adhered proteins from bacterial conditioning films via QCM-D/MALDI-ToF/MS. Anal Bioanal Chem. 2017;409(25):5965-74.
5. Welch RA, Burland V, Plunkett G, Redford P, Roesch P, Rasko D. Extensive mosaic structure revealed by the complete genome sequence of uropathogenic Escherichia coli. Proc Natl Acad Sci U S A. 2002;99(26):17020-4.
6. Mandakhalikar KD, Rahmat JN, Chiong E, Neoh KG, Shen L, Tambyah PA. Extraction and quantification of biofilm bacteria: method optimized for urinary catheters. Sci Rep. 2018;8(1):1-9.
7. Mas-Vinyals A, Gilabert-Porres J, Figueras-Esteve L, Borros S. Improving linking interface between collagen-based hydrogels and bone-like substrates. Colloids Surf B Biointerfaces. 2019;181:864-71.
8. Horna D, Ramírez JC, Cifuentes A, Bernad A, Borros S, González MA. Efficient cell reprogramming using bioengineered surfaces. Adv Healthc Mater. 2012;1(2):177-82.
9. Cifuentes A, Borros S. Comparison of two different plasma surface-modification techniques for the covalent immobilization of protein monolayers. Langmuir. 2013;29(22):6645-51.
10. Nguyen DHK, Pham VTH, Truong VK, Sbarski I, Wang J, Balcytis A. Role of topological scale in the differential fouling of Pseudomonas aeruginosa and Staphylococcus aureus bacterial cells on wrinkled gold-coated polystyrene surfaces. Nanoscale. 2018;10(11):5089-96.
11. Xiaoxue Z, Ling W, Erkki L. Superhydrophobic surfaces for the reduction of bacterial adhesion. RSC Adv. 2013;3:12003-20.
12. Anselme K, Davidson P, Popa AM, Giazzon M, Liley M, Ploux L. The interaction of cells and bacteria with surfaces structured at the nanometre scale. Acta Biomater. 2010;6(10):3824-46.
13. Mi G, Shi D, Wang M, Webster TJ. Reducing bacterial infections and biofilm formation using nanoparticles and nanostructured antibacterial surfaces. Adv Healthc Mater. 2018;7(13):1-23.
14. Marmur A. From hygrophilic to superhygrophobic: theoretical conditions for making high-contact-angle surfaces from low-contact-angle materials. Langmuir. 2008;24(14):7573-9.
15. Lee WK, Jung WB, Nagel SR, Odom TW. Stretchable superhydrophobicity from monolithic, three-dimensional hierarchical wrinkles. Nano Lett. 2016;16(6):3774-9.
16. Roach P, Shirtcliffe NJJ, Newton MII. Progess in superhydrophobic surface development. Soft Matter.

2008;4(2):224-40.
17. García-Bonillo C, Texido R, Reyes-Carmenaty G, Gilabert-Porres J, Borros S. Study of the human albumin role in the formation of a bacterial biofilm on urinary devices using QCM-D. ACS Appl Bio Mater. 2020;3(5):3354-64.
18. Damodaran VB, Murthy NS. Bio-inspired strategies for designing antifouling biomaterials. Biomater Res. 2016;20(1):18.
19. Montero L, Baxamusa SH, Borros S, Gleason KK. Thin hydrogel films with nanoconfined surface reactivity by photoinitiated chemical vapor deposition. 2009;26:399-403.
20. Artigues M, Gilabert-Porres J, Texido R, Borros S, Abella J, Colominas S. Analytical parameters of a novel glucose biosensor based on grafted PFM as a covalent immobilization technique. Sensors (Basel). 2021;21(12):1-15.
21. Lau KKS, Gleason KK. Particle surface design using an all-dry encapsulation method. Adv Mater. 2006;18(15):1972-7.
22. Jung WK, Koo HC, Kim KW, Shin S, Kim SH, Park YH. Antibacterial activity and mechanism of action of the silver ion in Staphylococcus aureus and Escherichia coli. Appl Environ Microbiol. 2008;74(7):2171-8.
23. Lansdown ABG. Silver in health care: antimicrobial effects and safety in use interactions between skin and biofunctional metals. Curr Probl Dermatol. 2006;33:17-34.
24. Kharisov B, Kharissova O, Ortiz-Mendez U. CRC Concise Encyclopedia of Nanotechnology. Boca Raton: CRC Press; 2016.
25. Lemire JA, Harrison JJ, Turner RJ. Antimicrobial activity of metals: mechanisms, molecular targets and applications. Nat Rev Microbiol. 2013;11(6):371-84.
26. Hagan EC, Donnenberg MS, Mobley HLT. Uropathogenic Escherichia coli. EcoSal Plus. 2009;3(2).
27. Terlizzi ME, Gribaudo G, Maffei ME. UroPathogenic Escherichia coli (UPEC) infections: virulence factors, bladder responses, antibiotic, and non-antibiotic antimicrobial strategies. Front Microbiol. 2017;8.
28. Ivanova EP, Hasan J, Webb HK, Gervinskas G, Juodkazis S, Truong VK. Bactericidal activity of black silicon. Nat Commun. 2013;4:1-7.
29. Linklater DP, Baulin VA, Juodkazis S, Crawford RJ, Stoodley P, Ivanova EP. Mechano-bactericidal actions of nanostructured surfaces. Nat Rev Microbiol. 2021;19(1):8-22.
30. Elbourne A, Chapman J, Gelmi A, Cozzolino D, Crawford RJ, Truong VK. Bacterial-nanostructure interactions: the role of cell elasticity and adhesion forces. J Colloid Interface Sci. 2019;546:192-210.
31. Sabir N, Ikram A, Zaman G, Satti L, Gardezi A, Ahmed A. Bacterial biofilm-based catheter-associated urinary tract infections: causative pathogens and antibiotic resistance. Am J Infect Control. 2017;45(10):1101-5.
32. Hetrick EM, Schoenfisch MH. Reducing implant-related infections: active release strategies. Chem Soc Rev. 2006;35(9):780-9.